PAPER

Check for updates

Synthesis and visible-light photocatalytic degradation of Ag₃PO₄/AgBr/hydroxyapatite ternary nanocomposites prepared from oyster shells

Sha Sha,[a] Lei Zhang,[a] Haijun Liu,[b] Jingdi Chen,[a] Yuju Che,[a] Fanbing Zhang[a] and Cui Song [ID] *[ab]

In this paper, a new type of Ag_3PO_4/AgBr/hydroxyapatite (HAP) composite was successfully prepared from oyster shells and silver nitrate by a hydrothermal method. The samples were characterized by scanning electron microscopy, X-ray photoelectron spectroscopy, electron spin resonance and other precision instruments, and their catalytic activity was characterized by visible light degradation of methylene blue (MB). The experimental results show that the Ag_3PO_4/AgBr/HAP photocatalyst has a nanoscale rod-like structure and excellent photodegradation performance. Although the content of Ag_3PO_4 or AgBr had a significant effect on the reaction activity, the effects did not all positively correlate, and only the appropriate ratio could produce an improved catalytic effect. The catalytic performance of the 1:1-Ag_3PO_4/AgBr/HAP composite was the best: complete degradation of MB was achieved within 40 min, and the reaction rate was 15 times that of Ag_3PO_4/AgBr. In the process of photocatalytic degradation, $\cdot O^{2-}$ and h^+ are the main active species involved in the reaction, and the synergistic catalysis of Ag_3PO_4, AgBr and HAP promotes the degradation rate.

1 Introduction

Dye wastewater is currently one of the most difficult industrial wastewaters to degrade, and its harm to the environment is becoming increasingly serious. How to treat it in a green and efficient way has become a research hotspot at present. Photocatalytic technology is an effective way to solve energy and environmental problems, and people are paying more attention to its application in wastewater treatment. Silver phosphate is a new and efficient visible light catalyst with a good development trend. However, the disadvantages of silver phosphate are that it is slightly soluble in water, prone to photocorrosion, and shows poor stability. The key to improving the activity and stability of silver phosphate is to explore and construct new and efficient silver phosphate composite photocatalysts. To this end, researchers have developed a series of complexes by combining materials with silver phosphate, such as CeO_2,[1] TiO_2,[2] AgX,[3] GO,[4] Ti_3C_2,[5] $CdWO_4$,[6] $BiVO_4$,[7] ZnO,[8] CuO[9] and g-C_3N_4.[10] The results show that an effective composite material is beneficial to the transfer of photogenerated carriers in the material and can effectively inhibit electron–hole recombination,[11] thus improving the photocatalytic activity of the material.

Silver bromide is a common semiconductor material. Ag_3PO_4/AgX (X = Cl, Br, and I) core–shell photocatalytic composites were synthesized by Bi *et al.*[12] using the ion exchange method and coating the surface of Ag_3PO_4 with a layer of AgX material with low water solubility. This material blocked the dissolution of Ag_3PO_4 in the system because of the lower water solubility of AgX coated on the outside of Ag_3PO_4 and solved the loss of Ag_3PO_4 in the system, thus contributing to the improvement of its stability.

Mariculture is one of the important ways to develop the global marine industry, and its production has doubled in recent years. In the use of marine shellfish, people pay more attention to the freshness of its shell rather than the use of its shell. Therefore, the mountains of shells not only cause a waste of resources but also cause serious environmental pollution and threaten human health. How to make full use of these natural resources, reduce environmental pollution and simultaneously obtain high-value products is a problem facing all countries in the world. To solve this problem, our research group prepared a series of hydroxyapatite (HAP, $Ca_{10}(PO_4)_6(OH)_2$) materials with different morphologies (including nanorods,[13] prism-like crystals,[14] microspheres,[15] *etc.*) from discarded oyster shells or abalone shells, which were used in biological materials and bone repair materials and achieved good results. However, the use as a catalyst carrier in the field of visible light catalysis is seldom reported.

[a]Marine College, Shandong University, Weihai 264209, China. E-mail: songcui@sdu.edu.cn

[b]Rushan Huaxin Foodstuffs Co.,Ltd, Weihai 264509, China

In this study, HAP nanorods were successfully prepared from oyster shells and then combined with Ag_3PO_4 and AgBr to produce a series of Ag_3PO_4/AgBr/HAP photocatalysts. This kind of material is not only expected to obtain a better catalytic effect but can also take into account the reuse of waste and further promote the sustainable development of green, clean and efficient production modes. This experiment not only provides a theoretical basis for the design of efficient catalysts for wastewater treatment but also provides a solution for the high value utilization of shells in coastal areas of the world.

2 Experimental materials and methods

2.1 The raw material

Oyster shells came from a seafood market in Weihai City, Shandong Province. The following reagents were purchased: glacial acetic acid (AR), Tianjin Fuyu Fine Chemical Co., Ltd.; phosphoric acid (AR), Yantai Shuangshuang Chemical Co., Ltd.; diamine hydrogen phosphate (AR), Tianjin Zhiyuan Chemical Reagent Co., Ltd.; ammonia (AR), Yantai Sanhe Chemical Reagent Co., Ltd; silver nitrate (AR) and methylene blue (AR), Sinopharm Chemical Reagents Co., Ltd.; anhydrous ethanol (AR), Tianjin Kaixin Chemical Industry Co., Ltd.; sodium bromide (AR), Tianjin Beitianyi Chemical Reagent Factory; and urea (AR), Tianjin Beichen Founder Reagent Factory. The water used in this experiment was superpure water made in the laboratory.

2.2 Preparation of materials

Preparation of HAP. The HAP in this paper was prepared by a hydrothermal method. Oyster shells were washed, crushed and dissolved in 10% acetic acid, and the filtrate was retained. 0.3 mol L^{-1} $(NH_4)_2HPO_4$ solution was added dropwise at the molar ratio of Ca/P = 1.67, the pH of the solution was adjusted to 9–10 with ammonia. Then, the solution was transferred to the reaction kettle and placed in a 160 °C thermostatic drying oven for 8 h. The product was washed with water and anhydrous ethanol, centrifuged and dried to produce HAP.

Preparation of photocatalyst. (1) Preparation of Ag_3PO_4: first, 0.5372 g of $Na_2HPO_4\cdot12H_2O$ and 0.5096 g of $AgNO_3$ were dissolved in water, then the $AgNO_3$ solution was dropped into the Na_2HPO_4 solution and stirred evenly. The mixture was left to stand, separated and dried to obtain Ag_3PO_4. (2) Preparation of

AgBr: 0.3087 g of NaBr and 0.5096 g $AgNO_3$ were dissolved in water, and then the NaBr solution was added into the $AgNO_3$ solution dropwise. The solid was collected and dried to obtain AgBr sample. (3) Preparation of Ag_3PO_4/AgBr: similar to the preparation of Ag_3PO_4, 0.1029 g of NaBr was added after dropping $AgNO_3$ into the solution. The following steps were the same as those for Ag_3PO_4, and finally, the Ag_3PO_4/AgBr sample was obtained. (4) Preparation of Ag_3PO_4/AgBr/HAP: 1 g of HAP carrier was dispersed in water to form a suspension, and $AgNO_3$ and NaBr of different proportions were dissolved in water and then dropped into the suspension. A series of composite catalysts with a certain mixture ratio were obtained after stirring and then dried at 100 °C for 8 h. The preparation process of the material is shown in Fig. 1, and the mass compositions of $AgNO_3$, NaBr and HAP are shown in Table 1.

2.3 Testing and characterization

Sample characterization. The structure and crystallinity of the samples were analyzed by X-ray powder diffraction (XRD, Rigaku, UltimaIV). Scanning electron microscopy (SEM, FEI, Nova Nanosem 450) and high-resolution transmission electron microscopy (HRTEM, JEOL, JEM-2100) were used to analyze the microstructures of the samples. Elemental analysis of samples by means of energy dispersive spectrometry (EDS, OXFORD, X-Max^{N}50). The specific surface area of the material was measured by an surface area and porosimetry analyzer (Micromeritics ASAP 2460). The composition and chemical states of the samples were determined by X-ray photoelectron spectroscopy (XPS, Thermo Fisher Scientific, Nexsa). The light absorption properties of the materials were analyzed by a ultraviolet-visible diffuse reflectance spectroscopy (UV-vis DRS, Shimazu, SolidSpec-3700). The electron spin resonance (ESR) signal of $^\cdot O^{2-}$ (trapped by 5,5-dimethyl-1-pyrroline-n-oxide (DMPO)) and h^+ (trapped by 2,2,6,6-tetramethyl-1-piperidinyloxy (TEMPO)) were measured by a Brooke A300 spectroscopy system.

Photocatalytic performance test. The degradation reaction of methylene blue (MB) solution under simulated sunlight irradiation was used as a model to evaluate the activity of different photocatalysts. The reaction was carried out in a photocatalytic reactor. The light source was a 500 W Xe lamp (λ = 300–800 nm). The catalyst (0.35 g) was added to 250 mL of 10 mg L^{-1} MB solution, and the sample was tested at intervals of 10–20 min after stirring in the dark for 40 min. After centrifugation, the absorbance of the solution at 664 nm was measured by a UV-vis

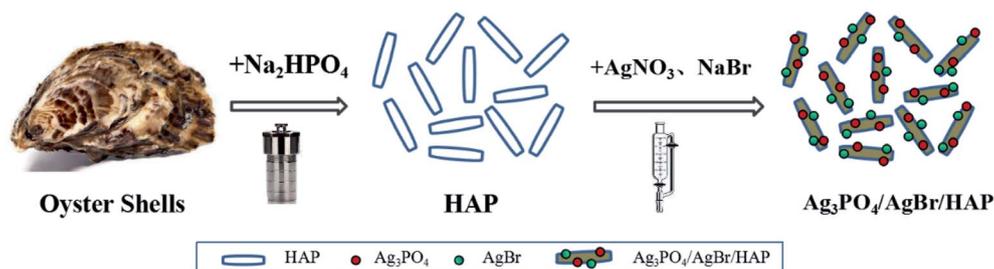**Fig. 1** The preparation process of Ag_3PO_4/AgBr/HAP.

Table 1 Quality ratio of different raw materials

Sample	Mass of AgNO$_3$/g	Mass of NaBr/g	Mass of HAP/g
Ag$_3$PO$_4$	0.51	0	0
AgBr	0.51	0.309	0
Ag$_3$PO$_4$/AgBr	0.51	0.103	0
1:4-Ag$_3$PO$_4$/AgBr/HAP	0.25	0.0515	1
1:2-Ag$_3$PO$_4$/AgBr/HAP	0.50	0.103	1
1:1.4-Ag$_3$PO$_4$/AgBr/HAP	0.70	0.154	1
1:1-Ag$_3$PO$_4$/AgBr/HAP	1	0.206	1
1:1-Ag$_3$PO$_4$/0.5AgBr/HAP	1	0.103	1
1:1-Ag$_3$PO$_4$/2AgBr/HAP	1	0.412	1
1:1-Ag$_3$PO$_4$/4AgBr/HAP	1	0.824	1

spectrophotometer (Hitachi, U-3900H), and the degradation curve with time was obtained.

Free radical capture experiment. Similar to the above photocatalytic performance test, a free radical capture agent was added in the above experimental process to investigate its influence on the degradation performance of MB. The trapping agents were isopropanol (IPA, ˙OH trapping agent), 1,4-benzoquinone (BQ, ˙O^{2-} trapping agent) and EDTA-2Na (h$^+$ trapping agent).

3 Results and discussion

3.1 Phase structure and morphology

To clarify the chemical composition of the material, we performed XRD analysis on the material. Fig. 2a shows the XRD patterns of HAP, Ag$_3$PO$_4$, AgBr, Ag$_3$PO$_4$/AgBr and 1:1-Ag$_3$PO$_4$/AgBr/HAP. Among them, the hydroxyapatite synthesized by oyster shells completely corresponds to the HAP standard spectrum (PDF#09-0432) card,[16,17] and the peak shape is sharp without impurity peaks, indicating that the HAP synthesized by this method is of high purity and good crystallinity. Similarly, the strong diffraction peaks of Ag$_3$PO$_4$ at $2\theta = 33.29°$ and $36.59°$ correspond to the (210) and (211) crystal planes of Ag$_3$PO$_4$ (PDF#06-0505).[18,19] The strong diffraction peaks at $2\theta = 30.960°$

and $44.346°$ are the characteristic peaks of the (200) and (220) crystal planes of AgBr (PDF#06-0438),[20–22] respectively. In addition to the strong signal peaks of Ag$_3$PO$_4$ and AgBr, the diffraction peaks of the HAP (002) and (211) crystal planes ($2\theta = 25.88°$ and $31.77°$) also appear in the spectra of Ag$_3$PO$_4$/AgBr/HAP. According to Fig. 2a, all four materials have sharp characteristic peaks, good crystallization degrees and no other heteropeaks, indicating that the experimental method can synthesize samples with high purity and crystallinity. Fig. 2b shows the XRD patterns of Ag$_3$PO$_4$/AgBr/HAP composites with different ratios. In this figure, the peak positions of different materials remain basically the same, and only the peak strength shows regular changes. With increasing silver content, the characteristic peak strength of silver phosphate increases. Similarly, when the silver content is fixed, the characteristic peak of silver bromide increases with increasing bromine content. This indicates that silver and bromine were loaded on the HAP carrier in the forms of Ag$_3$PO$_4$ and AgBr, respectively, during the preparation process. In addition, with the increase in raw materials, the content of Ag$_3$PO$_4$ or AgBr in the material also increased. All these phenomena indicate that HAP prepared from oyster shells is a carrier suitable for the loading of active components, and it has a good loading effect on both Ag$_3$PO$_4$ and AgBr.
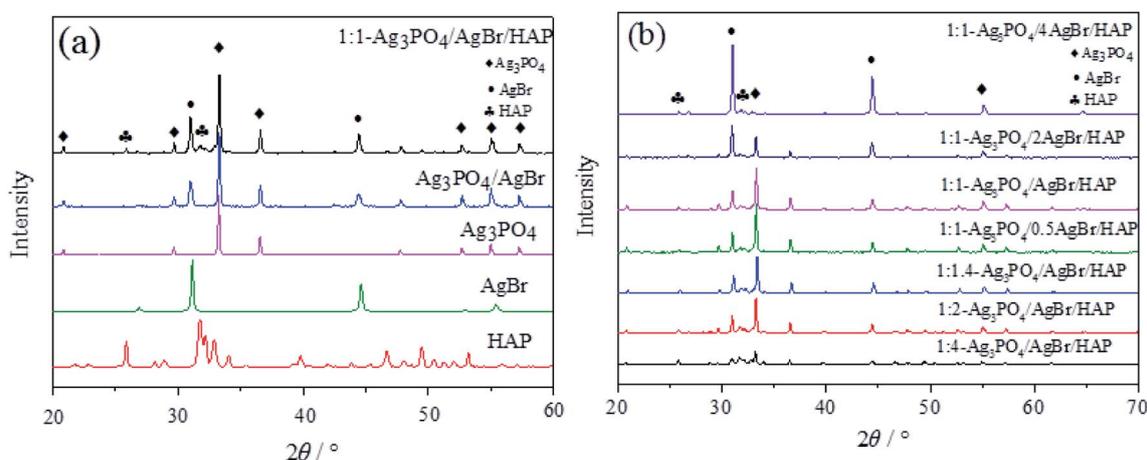

Fig. 2 XRD patterns of different samples: (a) different silver content; (b) different bromine content.

Fig. 3 shows electron microscopy images and energy spectra of different samples. Fig. 3a shows the HRTEM image of HAP synthesis from oyster shells, in which regular HAP nanorods can be clearly identified. The length is approximately 50–100 nm, and its width is approximately 40–50 nm. SEM images of Ag_3PO_4, AgBr and Ag_3PO_4/AgBr are shown in Fig. 3b–d, respectively. These materials have similar morphologies, presenting a circular cake shape with a particle size of approximately 200–500 nm, and the particles are stacked together and form certain holes. Fig. 3e–g shows the SEM images of three different Ag_3PO_4/AgBr/HAP composites: 1:2-Ag_3PO_4/AgBr/HAP (Fig. 3e), 1:1-Ag_3PO_4/AgBr/HAP (Fig. 3f) and 1:1-Ag_3PO_4/2AgBr/HAP (Fig. 3g). The SEM images of the three composites showed that the nanorod-like structure of HAP was maintained. With the doubling of silver or bromine loading, the morphology

of the material surface did not change significantly. The surface of the material was relatively smooth, and there was no aggregation of the active components. These results indicate that Ag_3PO_4 and AgBr can be uniformly dispersed in HAP nanorods without disrupting the composition and structure of HAP. The HRTEM diagram of the 1:1-Ag_3PO_4/AgBr/HAP material is shown in Fig. 3h–j. There are 0.817 nm, 0.245 nm and 0.288 nm diffraction patterns in the composite material, which correspond to the (100) plane of HAP, (211) plane of Ag_3PO_4 and (200) plane of AgBr, respectively. These results are consistent with the XRD conclusion from Fig. 1. The EDS mapping image (Fig. 2k) of Fig. 2j shows a homogenous distribution of the major elements such as silver and bromine in the composite. The results distinctly indicate that the Ag_3PO_4 and AgBr nanoparticles were dispersed on the surface of HAP, revealing that
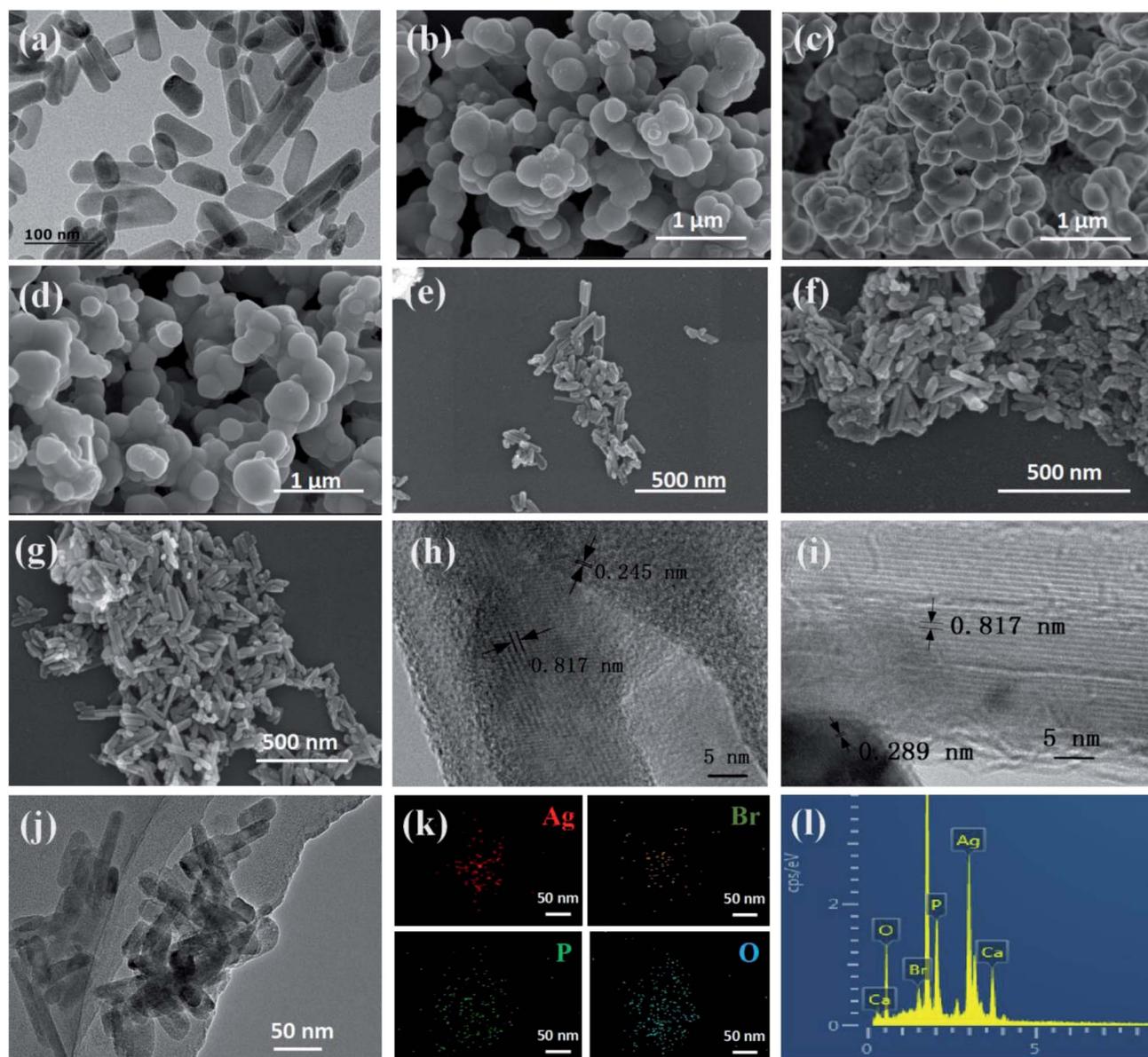

Fig. 3   HRTEM images of HAP (a); SEM images of Ag_3PO_4 (b); SEM images of AgBr (c); SEM images of Ag_3PO_4/AgBr (d); SEM images of Ag_3PO_4/AgBr/HAP (e–g); HRTEM images of Ag_3PO_4/AgBr/HAP (h–j); EDS mapping images (k) and EDS spectrum (l) of Ag_3PO_4/AgBr/HAP.

Fig. 5 UV-vis absorbance spectra (a) and Tauc plots (b) of the samples; N_2 adsorption and desorption isotherms of Ag_3PO_4/AgBr/HAP composites (c).

degradation occurred. As the figure shows, although HAP showed weak adsorption of MB during the dark treatment, the adsorbed MB was desorbed under visible light within 20 min. This result indicates that HAP has no ability to degrade MB under visible light. However, for Ag_3PO_4, AgBr and Ag_3PO_4/AgBr, the degradation rates of MB at 120 min were 61.69%, 39.82% and 54.98%, respectively. Besides, compared with the Ag_3PO_4/HAP catalyst, the Ag_3PO_4/AgBr/HAP catalyst showed stronger photodegradation performance when the light source was turned on (Fig. 6b). And when the bromine content is fixed, the catalytic performance of the composite steadily improves with increasing Ag_3PO_4/AgBr content. Among the four composite materials with different ratios, the 1:1-Ag_3PO_4/AgBr/HAP material showed better catalytic activity. The degradation rate reached 97.63% after 40 min, and MB was completely degraded. However, when the silver content was fixed, the photocatalytic

performance of the composites did not increase with increasing bromine content, as shown in Fig. 6c. In this figure, the adsorption capacity of the material for MB in the dark was improved with increasing bromine content. However, there was no similar trend in the catalytic activity of MB under visible light. In particular, 1:1-Ag_3PO_4/0.5AgBr/HAP and 1:1-Ag_3PO_4/AgBr/HAP with lower bromine contents showed better visible light degradation activity, with degradation rates of 97.48% and 97.63% at 40 min, resp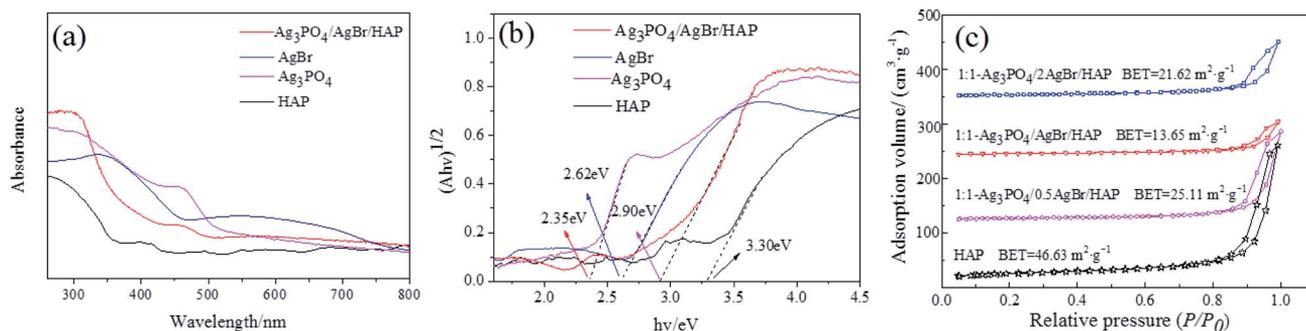ectively. The degradation time of Ag_3PO_4/HAP composites was 10 min shorter than that of Ag_3PO_4/HAP composites previously reported by our research group.[13] When the bromine content increased 2 to 4 times, the degradation rates of the composites at 40 min were only 81.07% and 59.88%, respectively. Similarly, the line fitting of the photocatalytic kinetics of different materials (Fig. 6d) shows that the composite material with a low bromine content has a better
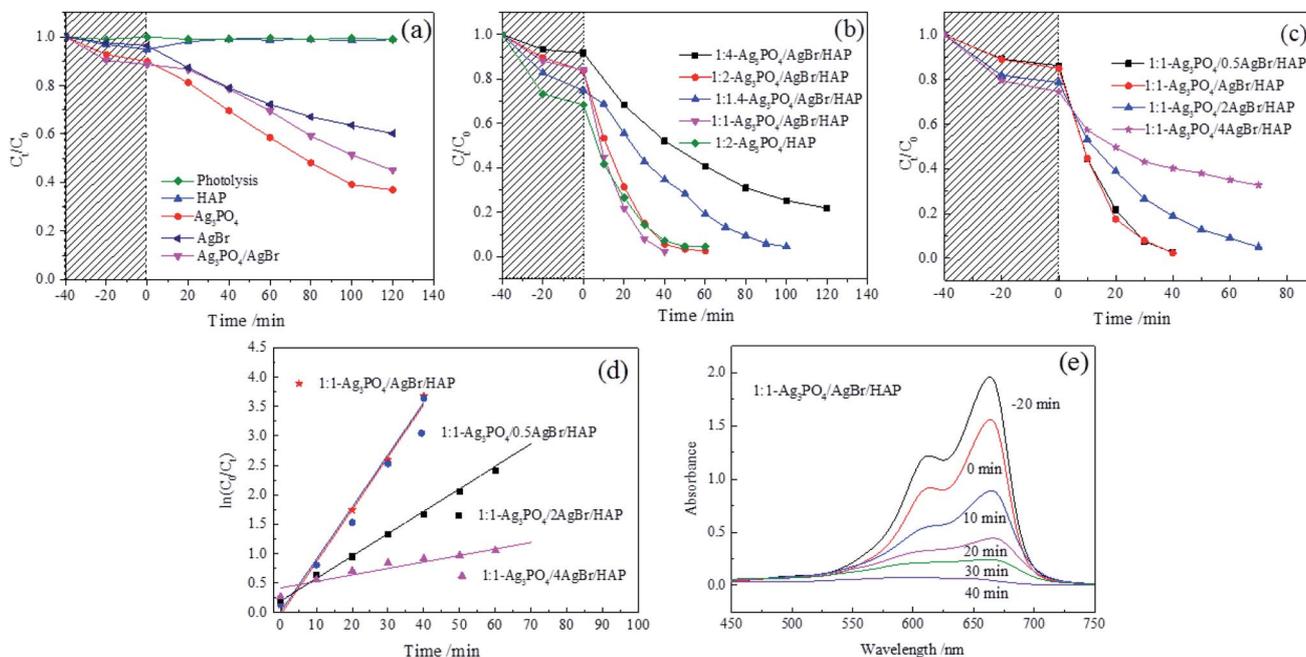

Fig. 6 Degradation curves of different samples (a–c); photocatalytic kinetics of different materials (d); UV-vis absorption spectrum of MB solution (e).
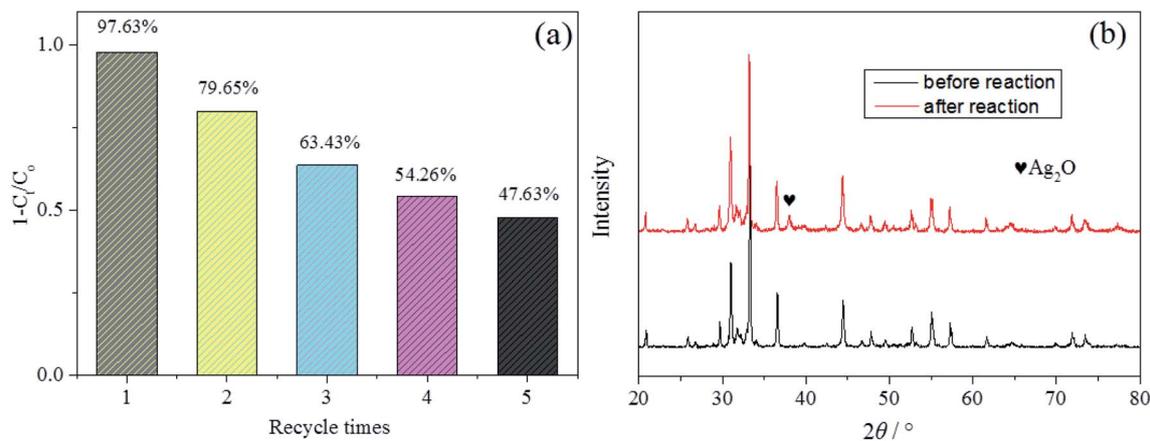
Fig. 7 Cycling runs of the composite for MB degradation (a); XRD patterns of the composite after five cycle degradation (b).

degradation rate, which is 12 times and 15 times that of the Ag_3PO_4 and $Ag_3PO_4/AgBr$ samples, respectively. In other words, the photocatalytic activity does not increase with increasing Br addition, but an appropriate ratio must be maintained. Moreover, during the experiment, we also found an obvious phenomenon: with increasing bromine content, the composite material is more inclined to adhere to the inner wall of the reaction vessel during the reaction process. Therefore, we believe that after adding bromine, the adsorption performance of the material is enhanced so that more methylene blue is adsorbed in the dark reaction stage. However, on the other hand, this strong adsorption capacity makes it difficult for MB to desorb, which hinders the redox reaction between MB and active radicals, leading to a decrease in its activity. Only when the catalyst and MB reach a proper equilibrium of adsorption and desorption can the reaction be carried out efficiently. This is also one of the reasons why the $1:1-Ag_3PO_4/AgBr/HAP$ material with a smaller specific surface area shows a higher catalytic effect. Fig. 6e shows the UV-vis absorption spectrum of MB solution in the reaction. The figure shows that the absorption peak of MB at 664 nm gradually weakened until it disappeared, indicating that MB was not transformed into other substances but underwent a thorough photodegradation reaction.

Five successive cyclic photocatalytic degradation experiments using the $Ag_3PO_4/AgBr/HAP$ were carried out to check the photocatalytic stability and durability of the prepared

photocatalyst and the result obtained were depicted in Fig. 7a. The cyclic results exhibited an reduction in the photodegradation ability after five consecutive degradation cycles of dye molecules. Although the stability of the sample still needs to be improved, the stability of the material is indeed improved 6% in the third cycle experiment compared with the previously reported two-component catalyst without AgBr.[33] This indicates that the addition of AgBr is not only beneficial to improve the photodegradation activity of MB, but also to improve the stability of the material. To evaluate the structural stability, the crystalline structures of $1:1-Ag_3PO_4/AgBr/HAP$ before and after experiments were studied (Fig. 7b). As shown in the figure, there is no significant difference, except the weak little peaks at $38.07°$, which is ascribed to Ag_2O (JCPDS-PDF #43-0997), indicating that a small amount of Ag_3PO_4 was converted to Ag_2O after cycle degradation. And this conversion resulted in the decrease of photocatalyst activity.

3.4 Photocatalytic mechanism

To elucidate the internal mechanism of the degradation of MB by $Ag_3PO_4/AgBr/HAP$ composites, we explored the main free radical species in the photocatalytic process through free radical capture experiments. A comparison of the degradation rates of materials without trapping agents or with 1 mmol trapping agents is shown in Fig. 8a. The figure shows that the
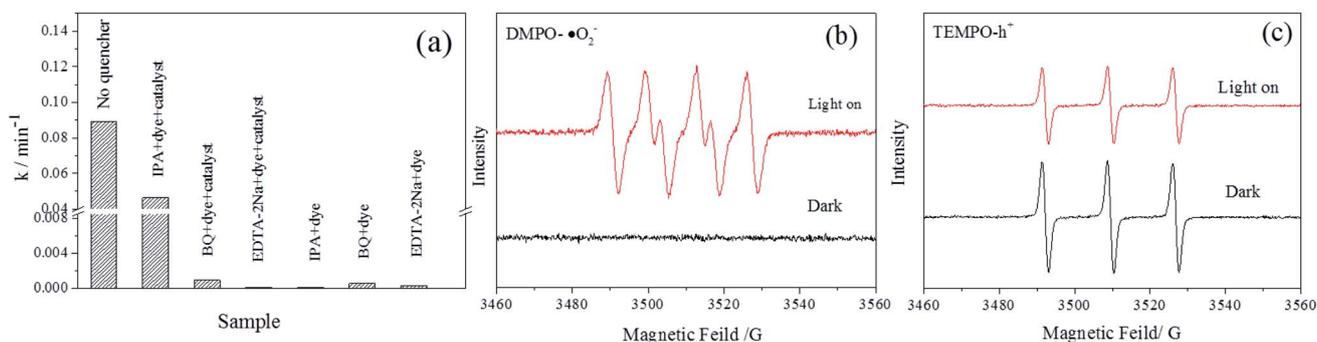

Fig. 8 Free radical capture test (a) and ESR signals (b and c) of $Ag_3PO_4/AgBr/HAP$.

catalytic activity of the composite material decreases to a certain extent after the addition of IPA, and the reaction rate decreases from 0.08929 min^{-1} to 0.04637 min^{-1}, indicating that some of the ·OH may be involved in the photocatalytic process. However, when BQ and EDTA-2Na were added, the degradation ability of MB was completely lost, and the reaction rate was extremely weak, which indicated that ·O^{2-} and h^+ were the main active species involved in the photocatalytic degradation of the 1:1-Ag_3PO_4/AgBr/HAP materials.[34] To verify this hypothesis, we performed ESR tests on the material, and the test results are shown in Fig. 8b and c. In Fig. 8b, compared with the dark condition, 6 characteristic signal peaks of DMPO-·O^{2-} were detected after the visible light was turned on.[35] Fig. 8c shows the TEMPO-h^+ signal of the composite material after dark and light irradiation. When the xenon lamp was turned on, h^+ generated after excitation of the photocatalyst quenched the electrons in TEMPO, resulting in weak electron signals. Therefore, the above experiments all indicate that ·O^{2-} and h^+ do exist in the reaction process after the material is stimulated by light, which is consistent with the results of the free radical capture test. Therefore, ·O^{2-} and h^+ are the main radical species involved in the degradation of MB in this reaction system.[36]

Based on the above characterization and degradation experiments, we deduced the photocatalytic mechanism of the Ag_3PO_4/AgBr/HAP composites, as shown in Fig. 9. In the Ag_3PO_4/AgBr/HAP ternary composite catalyst, the main active components of the material are Ag_3PO_4 and AgBr. HAP, as the substrate, also plays an important role in photocatalytic reactions. For the semiconductor Ag_3PO_4, the band gap is 2.4 eV, and AgBr is 2.6 eV.[12] When excited by visible light, electrons in the valence band of Ag_3PO_4 and AgBr can be excited and jump to the conduction band, making the conduction band and valence band generate photogenerated electrons and holes, respectively. The electrons in the AgBr conduction band can be transferred to the Ag_3PO_4 conduction band due to the matching of the two bands.[37] In contrast, the holes in the valence band were transferred from Ag_3PO_4 to AgBr and directly involved in the oxidation reaction of methylene blue degradation. Normally, due to the more negative potential of O_2/·O^{2-}(-0.33 V vs. NHE), the photo-generated electrons tended to in situ reduce Ag^+ to metallic Ag rather than generated the superoxide

radicals. However, from the free radical capture experiment and ESR test, we confirmed that the composite did produce superoxide radicals under light, and it played an important role in the process of photocatalytic reaction. We speculate that the production of superoxide radical is related to the oxygen vacancy in phosphate group of HAP.[38] It is reported that the oxygen vacancy on the surface of the material is conducive to the adsorption of O_2 molecules, and the foreign O_2 can be adsorbed on the oxygen vacancy in the form of superoxide state.[39] And the vacancy on HAP might act as a charge transmission bridge to made the electrons on the CB of Ag_3PO_4 transfer to HAP support due to electro-conductivity resulted from the alternation in electron state of surface phosphate group under light irradiation.[40,41] Therefore, under visible light irradiation, the silver-series material will generate photogenerated electrons and holes in the conduction band and valence band, respectively, after irradiation. The photogenerated electrons of AgBr first migrate to Ag_3PO_4 and then transfer to HAP together with electrons in the conduction band of Ag_3PO_4. The accumulated electrons on the HAP were easily trapped by the adsorbed O_2 on the vacancies to form superoxide radical (·O^{2-}), and then took part in the photooxidation. When the photoexcited electrons gradually accumulate on HAP, the holes in the valence band of Ag_3PO_4 transfer to the valence band of AgBr and become another reaction species involved in the photocatalytic reaction. This effective transfer mode can promote the rapid separation of electron–hole pairs and reduce the probability of carrier recombination in the material. The synergistic catalysis of the three can improve the overall photocatalytic performance of the material.

4 Conclusion

In this paper, a series of Ag_3PO_4/AgBr/HAP nanorod-like composites were prepared by loading silver and bromide ions on hydroxyapatite (HAP) prepared from oyster shells. After characterization, it was found that the purity of each component in the composite was high, and the nanostructure of HAP was maintained. The catalytic activity of the materials also changed with the different loading amounts. Among them, the degradation performance of the 1:1-Ag_3PO_4/AgBr/HAP composite was the best, and the complete degradation of methylene blue was achieved in 40 min. This indicates that it is feasible to use natural oyster shells as raw materials to prepare photocatalysts for pollutant degradation in this study. This method not only reduces the cost and achieves a better catalytic effect but also provides a new solution for the high-value utilization of oyster shells in global coastal areas. Therefore, this new mode of utilizing clean energy from solid waste to treat organic pollution wastewater will be one of the important directions of photocatalytic development in the future.

Fig. 9 Photocatalytic mechanism of Ag_3PO_4/AgBr/HAP composites.

Author contributions

C. Song contributed to the conception of the study and wrote the manuscript; S. Sha performed the experiment and wrote the manuscript; L. Zhang, Y. J. Che and F. B. Zhang contributed
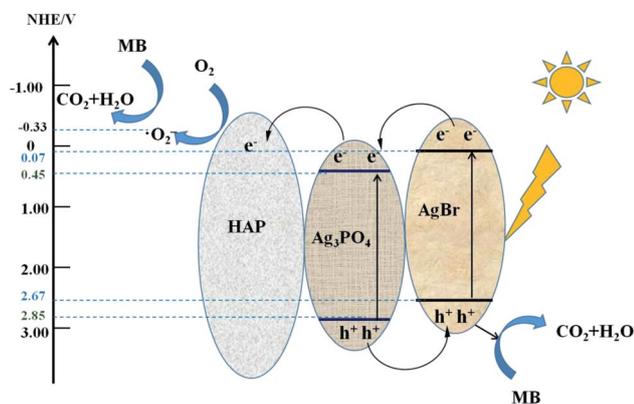
significantly to data analysis; H. J. Liu and J. D. Chen helped perform the analysis with constructive discussions. All coauthors contributed to the discussion, interpretation, and writing.

Conflicts of interest

The authors declare no competing financial conflict of interests among the coauthors and other researchers.

Acknowledgements

References

1 B. Borjigin, L. Ding, H. Q. Li, et al. A solar light-induced photo-thermal catalytic decontamination of gaseous benzene by using Ag/Ag$_3$PO$_4$/CeO$_2$ heterojunction, Chem. Eng. J., 2020, 402, 126070.

2 Q. Guan, S. Khan, Z. H. Wang, et al. The preparation, characterization of TiO$_2$-x/Ag$_3$PO$_4$ heterojunctions with enhanced photocatalytic visible-light performance, J. Alloys Compd., 2021, 852, 156947.

3 L. Zhu, W. Zhang, L. Chen, et al. A novel ternary visible-light-driven photocatalyst AgCl/Ag$_3$PO$_4$/g-C3N4: Synthesis, characterization, photocatalytic activity for antibiotic degradation and mechanism analysis, Catal. Commun., 2017, 100, 191–195.

4 H. Barzegar, M. A. Zahed and V. Vatanpour, Antibacterial and antifouling properties of Ag$_3$PO$_4$/GO nanocomposite blended polyethersulfone membrane applied in dye separation, Journal of Water Process Engineering, 2020, 38, 101638.

5 B. Sun, F. A. Tao, Z. X. Huang, et al. Ti$_3$C$_2$ MXene-bridged Ag/Ag$_3$PO$_4$ hybrids toward enhanced visible-light-driven photocatalytic activity, Appl. Surf. Sci., 2020, 535, 147354.

6 C. Zhang, L. Wang, F. Yuan, et al. Construction of p–n Type Ag$_3$PO$_4$/CdWO$_4$ Heterojunction Photocatalyst for Visible-light-induced Dye Degradation, Appl. Surf. Sci., 2020, 534, 147544.

7 Y. F. Wang, J. Niu, X. Gao, et al. Synergetic tuning of photocatalytic activity and photostability of Ag$_3$PO$_4$ via yttrium doping, carbon quantum dots and BiVO4 for atenolol degradation, Appl. Surf. Sci., 2020, 533, 147458.

8 Y. Yu, B. Yao, Y. He, et al. Piezo-enhanced photodegradation of organic pollutants on Ag$_3$PO$_4$/ZnO nanowires using visible light and ultrasonic, Appl. Surf. Sci., 2020, 528, 146819.

9 A. M. Taddesse and M. Alemu, Enhanced photocatalytic activity of p–n–n heterojunctions ternary composite Cu$_2$O/ZnO/Ag$_3$PO$_4$ under visible light irradiation, J. Environ. Chem. Eng., 2020, 8(5), 104356.

10 N. S. Alhokbany, R. Mousa, M. Naushad, et al. Fabrication of Z-scheme photocatalysts g-C3N4/Ag$_3$PO$_4$/chitosan for the photocatalytic degradation of ciprofloxacin, Int. J. Biol. Macromol., 2020, 164, 3864–3872.

11 C. Tang, E. Liu, J. Wan, et al. Co$_3$O$_4$ nanoparticles decorated Ag$_3$PO$_4$ tetrapods as an efficient visible-light-driven heterojunction photocatalyst, Appl. Catal., B, 2016, 181, 707–715.

12 Y. Bi, S. Ouyang, J. Cao, et al. Facile synthesis of rhombic dodecahedral AgX/Ag$_3$PO$_4$ (X = Cl, Br, I) heterocrystals with enhanced photocatalytic properties and stabilities, Phys. Chem. Chem. Phys., 2011, 13(21), 10071–10075.

13 C. Song, L. H. Zhao, M. Y. Qi, et al. Hydrothermal Preparation and properties of Ag$_3$PO$_4$/HAP composite photocatalysts, Chinese Jouranl of Inorganic Chemistry, 2020, 36(3), 521–528.

14 Q. Li, Z. Wen, J. Chen, et al. Preparation of controllable hydroxyapatite nanoparticles with abalone shells, Mater. Lett., 2019, 236, 562–565.

15 H. Huang, M. Z. Du, J. D. Chen, et al. Preparation and characterization of abalone shells derived biological mesoporous hydroxyapatite microspheres for drug delivery, Mater. Sci. Eng., C, 2020, 113, 110969.

16 R. P. Singh, M. Singh, G. Verma, et al. Structural analysis of silver doped hydroxyapatite nanopowders by rietveld refinement, Trans. Indian Inst. Met., 2017, 70, 1973–1980.

17 U. Erdem, M. Dogan, A. Umetin, et al. Hydroxyapatite-based nanoparticles as a coating material for the dentine surface: An antibacterial and toxicological effect, Ceram. Int., 2020, 46(1), 270–280.

18 W. Zheng, W. L. Yang, G. W. He, et al. Facile synthesis of extremely small Ag$_3$PO$_4$ nanoparticles on hierarchical hollow silica sphere (HHSS) for the enhanced visible-light photocatalytic property and stability, Colloids Surf., A, 2019, 571, 1–8.

19 X. J. Chen, C. M. Yu, R. L. Zhu, et al. Photocatalytic performance and mechanism of Z-Scheme CuBi$_2$O$_4$/Ag$_3$PO$_4$ in the degradation of diclofenac sodium under visible light irradiation: Effects of pH, H$_2$O$_2$, and S$_2$O$_8$$^{2-}$, Sci. Total Environ., 2020, 711, 134643.

20 Z. N. Yu, M. M. Xu, Q. Wang, et al. One-step reduction synthesis of Ag/Ag$_3$PO$_4$/AgBr sub-micron composites for enhanced visible photocatalytic degradation of methyl orange, Mater. Res. Bull., 2018, 104, 149–154.

21 H. Katsumata, T. Hayashi, M. Taniguchi, et al. Highly efficient visible-light driven AgBr/Ag$_3$PO$_4$ hybrid photocatalysts with enhanced photocatalytic activity, Mater. Sci. Semicond. Process., 2014, 25, 68–75.

22 H. X. Shi, S. Z. Yang, C. Han, et al. Fabrication of Ag/Ag$_3$PO$_4$/WO$_3$ ternary nanoparticles as superior photocatalyst for phenol degradation under visible light irradiation, Solid State Sci., 2019, 960, 105967.

23 O. A. Laput, D. A. Zuza, I. V. Vasenina, et al. Effect of silver ion implantation on surface physicochemical properties of composite materials based on polylactic acid and hydroxyapatite, Vacuum, 2020, 175, 109251.

24 X. Rao, H. L. Dou, D. Long, *et al.* Ag_3PO_4/g-C_3N_4 nanocomposites for photocatalytic degradating gas phase formaldehyde at continuous flow under 420 nm LED irradiation, *Chemosphere*, 2020, **224**, 125462.

25 H. Zhu, D. G. Guo, H. Zang, *et al.* Enhancement of hydroxyapatite dissolution through structure modification by Krypton ion irradiation, *J. Mater. Sci. Technol.*, 2020, **381**, 148–158.

26 B. Boruah, R. Gupta, J. M. Modak, *et al.* Enhanced Photocatalysis and Bacterio-inhibition in Nb_2O_5 via Versatile Doping of Metal (Sr, Y, Zr, Ag): A Critical assessment, *Nanoscale Adv.*, 2019, **1**, 2748–2760.

27 L. W. Chen, S. J. Yang, Y. Huang, *et al.* Degradation of antibiotics in multi-component systems with novel ternary $AgBr$/Ag_3PO_4@natural hematite heterojunction photocatalyst under simulated solar light, *J. Hazard. Mater.*, 2019, **371**, 566–575.

28 L. S. Lu, Y. Zhang, Z. B. Yuan, *et al.* Easily fabricated HARCP/ HAP photocatalyst for efficient and fast removal of tetracycline under natural sunlight, *Chem. Eng. J.*, 2021, **412**, 128620.

29 N. Raeisi-Kheirabadi and A. Nezamzadeh-Ejhieh, A Z-scheme g-C_3N_4/Ag_3PO_4 nanocomposite : Its photocatalytic activity and capability for water splitting, *Int. J. Hydrogen Energy*, 2020, **45**(58), 33381–33395.

30 F. Puga, J. A. Navio and M. C. Hidalgo, Enhanced UV and visible light photocatalytic properties of synthesized $AgBr$/ SnO_2 composites, *Sep. Purif. Technol.*, 2021, **257**, 117948.

31 V. S. Bystrov, C. Piccirillo, D. M. Tobaldi, *et al.* Oxygen vacancies, the optical band gap (Eg) and photocatalysis of hydroxyapatite: Comparing modelling with measured data, *Appl. Catal., B*, 2016, **196**, 100–107.

32 J. F. Jin, M. Liu, L. H. Feng, *et al.* 3D Bombax-structured carbon nanotube sponge coupling with Ag_3PO_4 for tetracycline degradation under ultrasound and visible light irradiation, *Sci. Total Environ.*, 2019, **695**, 133694.

33 C. Song, M. Y. Qi, J. F. Liu, *et al.* Preparation of Ag_3PO_4/HAP composite photocatalyst and its efficient degradation of methylene blue, *Acta Mater. Compos. Sin.*, 2020, **37**, 1418–1425.

34 M. I. Shinger, A. M. Idris, S. Devaramani, *et al.* In situ fabrication of graphene-based Ag_3PO_4@$AgBr$ composite with enhanced photocatalytic activity under simulated sunlight, *J. Environ. Chem. Eng.*, 2017, **5**(2), 1526–1535.

35 S. Q. Huang, Y. G. Xu, T. Zhou, *et al.* Constructing magnetic catalysts with in-situ solid-liquid interfacial photo-Fenton-like reaction over Ag_3PO_4@$NiFe_2O_4$ composites, *Appl. Catal., B*, 2018, **225**, 40–50.

36 B. Q. Ju, F. Yang, K. Huang, *et al.* Fabrication, characterization and photocatalytic mechanism of a novel Z-scheme $BiOBr$/Ag_3PO_4@rGO composite for enhanced visible light photocatalytic degradation, *J. Alloys Compd.*, 2020, **815**, 151886.

37 H. R. Wang, L. Zou, Y. C. Shan, *et al.* Ternary GO/Ag_3PO_4/ $AgBr$ composite as an efficient visible-light-driven photocatalyst, *Mater. Res. Bull.*, 2018, **97**, 189–194.

38 H. Nishikawa, Surface changes and radical formation on hydroxyapatite by UV irradiation for inducing photocatalytic activation, *J. Mol. Catal. A: Chem.*, 2003, **206**, 331–338.

39 H. L. Nguyen, T. Q. Nguyen, W. A. Dino, *et al.* Effect of oxygen vacancy on the adsorption of O_2 on anatase TiO_2(001): A DFT-based study, *Surf. Sci.*, 2015, **633**, 38–45.

40 Y. Y. Chai, J. Ding, L. Wang, *et al.* Enormous enhancement in photocatalytic performance of Ag_3PO_4/HAP composite: A Z-scheme mechanism insight, *Appl. Catal., B*, 2015, **179**, 29–36.

41 Q. Chang, X. Meng, S. L. Hu, *et al.* Hydroxyapatite/N-doped carbon dots/Ag_3PO_4 composite for improved visible-light photocatalytic performance, *RSC Adv.*, 2017, **7**(48), 30191–30198.